

Entanglement Entropy of Causal Set de Sitter Horizons

Sumati Surya¹, Nomaan X¹, and Yasaman K. Yazdi^{2,3}

¹*Raman Research Institute, Sadashivnagar, Bangalore 560 080, India*

²*Theoretical Physics Group, Blackett Laboratory, Imperial College London,
SW7 2AZ, UK*

³*Department of Physics, 4-181 CCIS, University of Alberta, Edmonton AB,
T6G 2E1, Canada*

ssurya@rri.res.in, nomaan@rri.res.in, ykouchek@imperial.ac.uk

Abstract

de Sitter cosmological horizons are known to exhibit thermodynamic properties similar to black hole horizons. In this work we study causal set de Sitter horizons, using Sorkin's spacetime entanglement entropy (SSEE) formula, for a conformally coupled quantum scalar field. We calculate the causal set SSEE for the Rindler-like wedge of a symmetric slab of de Sitter spacetime in $d = 2, 4$ spacetime dimensions using the Sorkin-Johnston vacuum state. We find that the SSEE obeys an area law when the spectrum of the Pauli-Jordan operator is appropriately truncated in both the de Sitter slab as well as its restriction to the Rindler-like wedge. Without this truncation, the SSEE satisfies a volume law. This is in agreement with Sorkin and Yazdi's calculations for the causal set SSEE for nested causal diamonds in M^2 , where they showed that an area law is obtained only after truncating the Pauli-Jordan spectrum. In this work we explore different truncation schemes with the criterion that the SSEE so obtained obeys an area law.

1 Introduction

Cosmological horizons in de Sitter (dS) spacetime share several key features with black hole horizons [1–3], as first suggested in [4]. Classically, both can be associated with a temperature, as well as an entropy proportional to the horizon area based on a mathematical analogy with the laws of thermodynamics. Quantum mechanically, observers outside both horizons can detect thermal radiation characterised by the horizon temperature. However there are also key differences [5]. Most obvious is the fact that different observers in de Sitter have different corresponding horizons. Moreover, the thermality of dS radiation is not reflected in the stress energy tensor of the quantum state and is instead red-shifted by the expansion. Despite this, the entropy-area relationship is robust and can moreover be extended to all causal horizons [6].

The interaction of matter fields with black hole horizons also exhibits thermodynamic features. As in the case of a black body, incoming radiation is scattered into thermal

radiation at around the black hole temperature [7]. In [8] Sorkin proposed that the dominant contribution to black hole entropy can potentially come from the entanglement entropy (EE) of a non-gravitational field. This EE was defined using the reduced density matrix of the exterior region. An explicit calculation for a scalar field was carried out in [9] and seen to give rise to an area law after imposing a UV cutoff. An area dependence arises naturally from complementarity and is an important feature of EE. It has been shown to hold for a diverse range of quantum systems [10].

Numerous researchers have since studied the connection between EE and black hole entropy [11–14]. In [15] Jacobson suggested that the “species puzzle” can be resolved by showing that the renormalisation of the gravitational constant appearing in the Bekenstein-Hawking entropy is similarly species dependent. In recent years, the idea of holographic EE has gained considerable ground starting with the work of Ryu and Takayanagi [16]. The EE in dS was first calculated in [17] and shown to exhibit the area law relation, both for a free massive field theory using the dS Euclidean vacuum, as well as for strongly coupled field theories with holographic duals (see also [18]).

All these calculations of the EE use the density matrix specified on a partial Cauchy hypersurface Σ , with the entropy attributed to its spacetime domain of dependence $\mathcal{D}(\Sigma)$. However, it is desirable to define the EE in a more covariant language, since horizons are intrinsically spacetime in character. In [19] Sorkin proposed a spacetime EE, which we term the Sorkin Spacetime Entanglement Entropy or SSEE for short, defined for a Gaussian free scalar field theory. The SSEE between a globally hyperbolic subregion O in a globally hyperbolic compact¹ spacetime region \mathcal{M} and its causal complement is given by

$$\mathcal{S} = \sum_{\mu} \mu \ln |\mu| \quad (1)$$

where μ is the generalised eigenvalue

$$W_O(x, x')v = i\mu \Delta_O(x, x')v, \quad \Delta_O v \neq 0, \quad (2)$$

and $W_O(x, x')$ and $i\Delta_O(x, x')$ denote the restrictions to O of the Wightman function $W(x, x') = \langle 0|\phi(x)\phi(x')|0\rangle$, and the Pauli-Jordan function $i\Delta(x, x') = [\phi(x), \phi(x')]$, respectively. Recently this formula has been shown to be valid up to first order in perturbation theory for generic perturbations away from the free field Gaussian theory as well [20]; in this case the Gaussian free field correlation functions are replaced with their perturbation-corrected counterparts.

In [21] \mathcal{S} was calculated for nested causal diamonds in $d = 2$ continuum Minkowski spacetime \mathbb{M}^2 , $\mathbb{D}_{\ell}^2 \subset \mathbb{D}_L^2$, which are each the domain of dependence of nested spatial intervals of lengths $2\sqrt{2}\ell$ and $2\sqrt{2}L$, respectively, as shown in Figure 1. Rather than the Minkowski vacuum, the calculation of [21] used the covariantly defined Sorkin-Johnston (SJ) vacuum for free scalar fields [22, 23]. As in other calculations of EE, \mathcal{S} can be calculated in the continuum only after imposing a UV cutoff. The SJ vacuum offers the choice of a covariant cutoff in the eigenspectrum of the Pauli-Jordan operator $i\hat{\Delta}$ (the SJ spectrum), which is at

¹The compactness condition on \mathcal{M} is important in defining the SSEE, since the domain of the integral operator $i\hat{\Delta}$ is the space of compactly supported functions, while its range includes functions that are not of compact support.

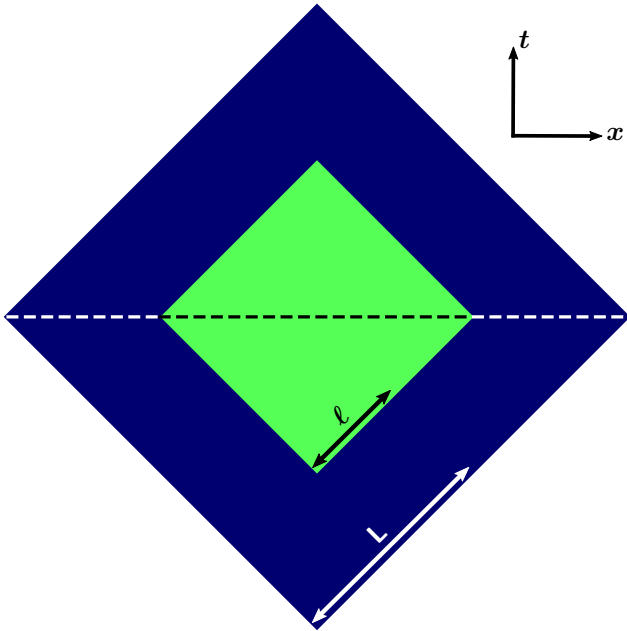


Figure 1: The causal completion or domain of dependence \mathcal{D} of two line segments, one contained within the other.

the heart of the SJ construction. Using this cutoff it was shown in [21] that the \mathcal{S} satisfies the expected $d = 2$ “area” law.

Since a causal set which is approximated by a continuum spacetime comes with a built-in covariant spacetime cutoff $1/\rho$, one might expect that the SSEE for a causal set doesn’t need further regularisation. While it is finite for a finite causal set, it was shown in [24] that the SSEE in the causal set version of the calculation in [21] obeys a spatial area law only after a suitable “double truncation” of the causal set SJ spectrum both in \mathbb{D}_L^2 and in \mathbb{D}_ℓ^2 . Without this, the SSEE follows a spacetime volume law and thus violates complementarity.

The double truncation used in [24] was motivated by comparing the SJ spectra of the continuum with that of the causal set in \mathbb{D}_L^2 . The latter possesses a characteristic “knee” at which the eigenvalues dramatically drop to small but non-zero values (see Figure 2). It is roughly around this knee that the discrete and continuum spectra begin to disagree. Importantly, while the formula for the SSEE (1) excludes solutions with strictly zero eigenvalues, it does not exclude those with finite *near* zero eigenvalues, which characterise the post-knee causal set SJ spectrum. These modes can be shown to contribute to large μ values in (1) which then dominate the SSEE. If we include eigenfunctions v that lie in the kernel of $i\Delta$ but not necessarily of W , this gives an infinite contribution to \mathcal{S} , since the equation can only be satisfied for $\mu \rightarrow \infty$ (this is also discussed in [25]). Thus, in the causal set, the contribution from a v which is *almost* in the kernel, i.e., $\|i\Delta v\| \approx 0$, lends itself to a very large (though finite) value of μ , and hence to a much larger SSEE.

Extending this work to gravitational horizons is of course very important, not least because causal sets provide a covariant UV cutoff, essential to the finiteness of EE. Calculating the SJ vacuum for a free scalar field in the causal set needs the proper identification of the

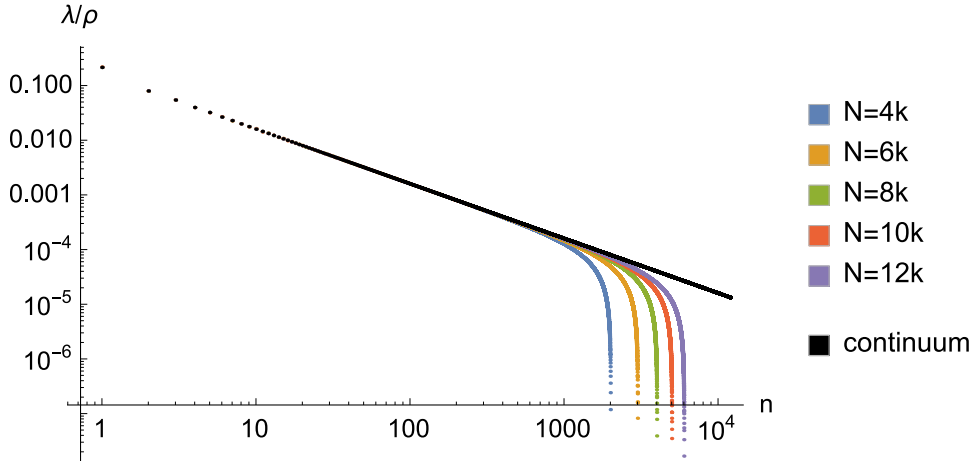


Figure 2: Log-log plot of the normalised SJ spectrum for the 2d causal diamond of side length $2L = 1/\sqrt{2}$, for both the continuum as well as for causal sets of size N . On the y-axis, λ refers to the SJ eigenvalue (see appendix B) and $1/\rho$ is the covariant volume cut-off coming from the causal set.

dimension dependent causal set retarded Green function [26]. While such an identification is not yet known for black hole spacetimes, it has been obtained for dS [27], which in turn gives us the ability to calculate the causal set dS SSEE. The causal set dS SJ vacuum was obtained in [28] and found to differ significantly from the known continuum α -vacua. In the continuum it is known that the latter are the only possible dS invariant vacua, which suggests that the causal set discretisation and/or the SJ prescription has a non-trivial effect on the QFT vacuum.

In this work we calculate the causal set SSEE for the dS horizon, for a conformally coupled, massless, free scalar field in dimensions $d = 2, 4$. We find that, as for nested causal diamonds in \mathbb{M}^2 , the SSEE obeys an area law only after a suitable double truncation, without which it follows a spacetime volume law. The truncation scheme used in [24] used the explicit analytic form of the SJ spectrum in the 2d flat spacetime causal diamond to motivate the truncation in the causal set SJ spectrum. The analytic form of the SJ spectrum is however not known more generally. In this work we motivate the choice of truncation scheme for the dS causal set SJ spectrum by requiring the causal set SSEE to satisfy an area law. As we will see, satisfying this criterion is quite non-trivial.

Section 2 provides a background for our work. In Section 2.1 we begin with a discussion of area laws and complementarity. We define the two complementary Rindler-like wedges in dS and the corresponding Bekenstein-Hawking area law which we might expect to recover from the SSEE. In Section 2.2 we set up the calculation of the SSEE in a finite causal set. In Section 2.3 we review the results of the calculation of SSEE for nested causal diamonds in \mathbb{M}^2 [24] and the critical role played by the double truncation procedure in obtaining the area law. In Section 2.4 we propose generalisations of the truncation scheme of [24] for general spacetimes, in the absence of analytic results on the SJ spectrum in the continuum.²

²The continuum SJ spectrum in the dS slab has been recently obtained [29], but not in the Rindler-like

In Section 3 we present the results of extensive numerical simulations for the causal set SSEE for dS_{2,4} horizons. Our investigations of different truncation schemes show that an area law compatible with the Bekenstein-Hawking entropy of the horizon is not easy to satisfy. Complementarity on the other hand is guaranteed, up to Poisson fluctuations, by the fact that the Rindler-like wedges are identical in the continuum. We present a few truncation schemes and discuss their relative merits. We end with open questions in Section 4. The Appendices contain some of the background material on the SJ vacuum as well as a calculation of the causal set SSEE for nested causal diamonds in M⁴, where finding a truncation that satisfies both an area law and complementarity has proven to be more non-trivial.

2 Preliminaries

2.1 Complementary Regions in Global dS

Let (\mathcal{M}, g) be a globally hyperbolic spacetime region and O a globally hyperbolic subregion $O \subset \mathcal{M}$. The SSEE of O is defined with respect to its causal complement O' , where $O' \subset O^c \subset \mathcal{M}$ such that $x \in O' \Leftrightarrow x$ is spacelike to O . Since (\mathcal{M}, g) is globally hyperbolic, so is O' and hence the EE of O' can also be defined with respect to O , which is *its* causal complement. O and O' are said to be *complementary* to each other, where we now use the term “complementarity” to denote causal complementarity. Figure 3 shows an example of a smaller causal diamond \mathbb{D}_ℓ^2 nested inside a larger one \mathbb{D}_L^2 in M². The complement O' to $O \sim \mathbb{D}_\ell^2$ is a union of two disconnected causal diamonds. In [21] and [24] the SSEE of O with respect to O' was calculated in the continuum and in the causal set, respectively. Note that in the standard definition the spatial complementary regions Σ_O and $\Sigma_{O'}$ are used to define EE, where Σ_O denotes a partial Cauchy hypersurface of the region O in Σ , a Cauchy hypersurface of (\mathcal{M}, g) . However, because O is globally hyperbolic, the “information content” of Σ_O is the same as that of O .

A feature of bipartite EE is that it satisfies complementarity, i.e., that the EE of O with respect to its complement O' is the same as that of O' with respect to O . This in turn implies the area law since the two complementary regions only share a spatial boundary separating them. The gross feature of this boundary is its “area” or $d - 2$ spatial volume, which means that the EE satisfies an area law.³ Conversely, a scaling of the EE with the spatial or spacetime volume of the region means that complementarity is not satisfied, since in general the volumes of O and O' can be unequal.

In dS, one wishes to calculate the SSEE between the two Rindler-like wedges which intersect at the bifurcate horizon. The dS metric is [31]

$$ds^2 = -d\tau^2 + l^2 \cosh^2(\tau/l) d\Omega_{d-1}^2, \quad (3)$$

where $-\infty < \tau < \infty$ and l is the dS radius. Using $\cosh(\tau/l) = \frac{1}{\cos T}$ it can alternatively be written as

$$ds^2 = \frac{l^2}{\cos^2 T} (-dT^2 + d\Omega_{d-1}^2), \quad (4)$$

wedge.

³The EE could also depend on the more detailed geometry of the boundary, but we will ignore this possibility in our work. See [30] for a discussion on this.

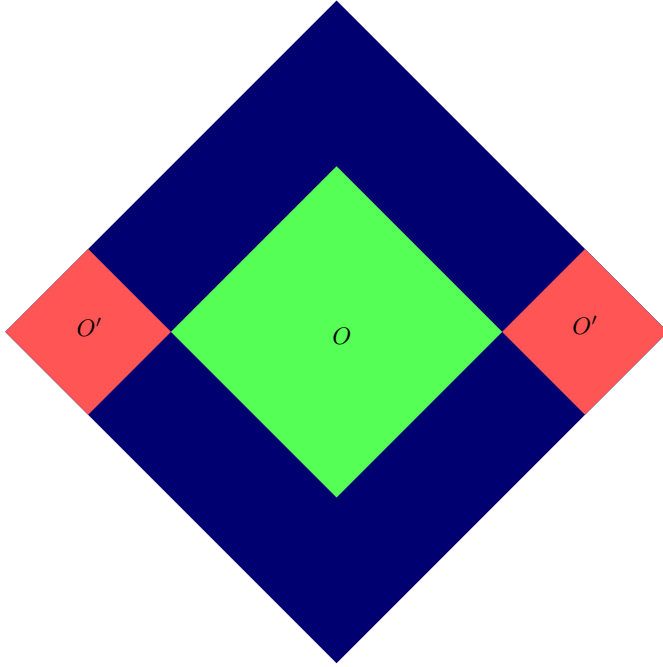


Figure 3: A nested causal diamond O and its complement O' in \mathbb{M}^2 .

where $-\pi/2 < T < \pi/2$, which is conformal to the round cylinder $S^{d-1} \times [-\pi/2, \pi/2]$. As shown in the conformal diagram in Figure 4, associated with any time-like observer o is a future/past horizon $\mathcal{H}_\pm = \partial(J^\pm(\gamma_o))$ where γ_o is the world line of o . The Rindler-like wedge $\mathcal{R}_o \equiv J^+(\gamma_o) \cap J^-(\gamma_o)$ has a boundary which intersects \mathcal{H}_+ and \mathcal{H}_- at a bifurcate horizon, whose area is $A = 4\pi l^2$ in 4d. Let us assume that the observer is at the south pole o_S . The Rindler-like wedge \mathcal{R}_{o_N} associated with its antipode at the north pole, o_N , is then the complement of \mathcal{R}_{o_S} . The SSEE we wish to calculate is from the entanglement between these two identical Rindler-like wedges, which should therefore also satisfy complementarity.

The EE for dS₂ should have the same form as that for flat space. It contains a logarithmic UV cutoff dependence and in the case with two boundaries is given by [10, 12]

$$S = \frac{1}{3} \ln\left(\frac{l}{a}\right) + b, \quad (5)$$

where a is a UV cutoff and b a non-universal constant. For dS₄, the entropy-area relation, which is the same as the Bekenstein-Hawking entropy, is expected to be [4, 32]

$$S = \frac{A}{\ell_p^2} = \frac{c^3}{4G\hbar} A = \pi l^2 \quad (\text{for } G = \hbar = c = 1). \quad (6)$$

It is with these formulae that we will compare our results and ask if the causal set SSEE we find can account for the expected behaviour. It is understood that when (6) is compared with the EE, the area of the entangled region in the EE is in units of the UV cutoff.

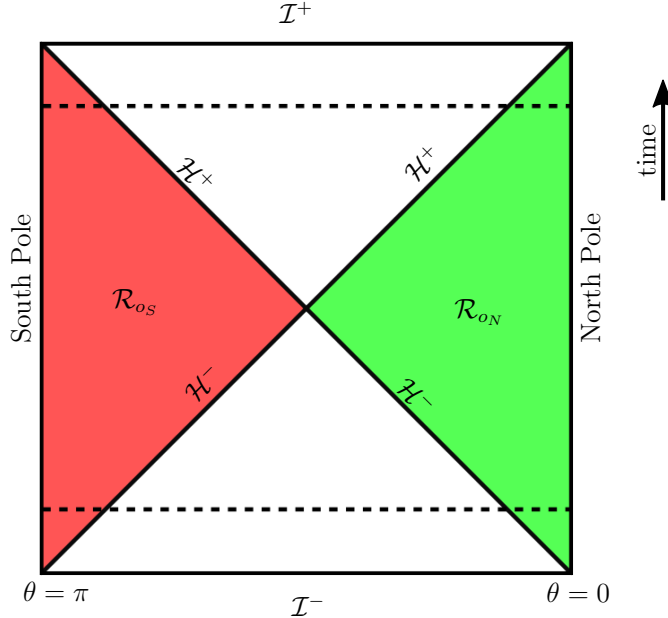


Figure 4: The entangled Rindler-like wedges in dS corresponding to observers at the north and south pole. The dashed lines correspond to the boundaries of the slabs we consider.

2.2 Causal Set SSEE

Next, we set up the calculation of the horizon SSEE in a causal set approximated by dS. We refer the reader to the literature on causal sets [33–35] and Appendix A for more details.

Given a finite volume V region of a globally hyperbolic spacetime (\mathcal{M}, g) , an ensemble of causal sets can be obtained from it via a Poisson sprinkling at density ρ , where the number of causal set elements N is a random variable whose average is given by

$$\langle N \rangle = \rho V. \quad (7)$$

Causal sets obtained from a sprinkling are said to be continuum-like, and we will denote this by $C \sim (\mathcal{M}, g)$. For a particular realisation C , we denote by C_O the sub-causal set approximated by the subregion $O \subset \mathcal{M}$, and its cardinality by N_O .

Since our calculations are numerical, we are limited by the size N and hence to finite volumes V of dS. As in [28] we pick a symmetric “slab” of dS with $T \in [-h, h]$, so that in 4d

$$V_{\text{slab}} = \frac{4\pi^2 l^4}{3} f(h), \quad f(h) = \tan h \left(\cos 2h + 2 \right) \sec^2 h. \quad (8)$$

The causal sets we obtain from this sprinkling therefore have finite N .

Before defining the causal set SSEE, it is useful to translate the continuum entropy-area relation to the discrete one, by identifying the UV cutoff as the discreteness length $\rho^{-1/d} = \sqrt[d]{V/N}$. Replacing ℓ_p in (6) with the causal set cutoff, we have in $d > 2$

$$\langle S^{(c)} \rangle = \rho^{\frac{2}{d}} \frac{A}{4}. \quad (9)$$

Using the slab volume (8) in dS₄, this translates into the discrete entropy

$$S^{(c)} = \frac{1}{2} \sqrt{\frac{3}{f(h)}} \sqrt{N}. \quad (10)$$

In $d = 2$, the discrete entropy is given by taking the cutoff a in (5) to be $\sqrt{\frac{1}{\rho}} = \sqrt{\frac{V}{N}}$. In dS₂, therefore, the discrete entropy should take the universal $d = 2$ form

$$S^{(c)} = \frac{1}{6} \ln N + b. \quad (11)$$

We now review the definition of the SSEE associated with a Gaussian scalar field on a causal set C . We begin with the discrete Pauli-Jordan function $i\Delta_C(x, x')$ which is the difference between the causal set retarded and advanced Green functions $G_{R,A}(x, x')$, for $x, x' \in C$, defined using the order relations in C . The SJ prescription then associates a unique state, or Wightman function $W_C(x, x')$ as the positive part of $i\Delta_C(x, x')$ (see Appendix B). Next, consider any causally convex subset $C_O \subset C$ and the restrictions $i\Delta_{C_O}(x, x')$, $W_{C_O}(x, x')$ of $i\Delta_C(x, x')$ and $W_C(x, x')$ to C_O . Importantly, although $W_C(x, x')$ is a pure state, this is not true of $W_{C_O}(x, x')$ which is not the positive part of $i\Delta_{C_O}(x, x')$. The simplest form⁴ that the causal set SSEE $S^{(c)}$ takes is then

$$\mathcal{S}^{(c)} = \sum_{\mu} \mu \ln |\mu|, \quad W_{C_O} \circ v = i\mu \Delta_{C_O} \circ v, \quad \Delta_{C_O} \circ v \neq 0, \quad (12)$$

where for $x \in C_O$, $A_{C_O} \circ v(x) \equiv \sum_{x' \in C_O} A(x, x')v(x')$. We will henceforth refer to the above equation and its continuum counterpart as the SSEE equation and v and μ as generalised eigenvectors and eigenvalues. Note that in adapting the continuum formula to the causal set, we have retained the strict requirement that v cannot lie in the kernel of Δ_{C_O} .

For a causal set with no continuum counterpart, there is no unique or “natural” choice of $G_{R,A}(x, x')$, and subsequently no unique SJ vacuum and SSEE. Since an area law for the SSEE is geometric, one expects such a relation to hold only for causal sets which admit a geometric interpretation, i.e., a continuum approximation. Thus, although the SSEE given by (12) can be calculated for any causal set along with a choice of $G_{R,A}(x, x')$, an area law makes sense only for continuum-like causal sets. By comparing with the continuum, the causal set Green functions $G_{R,A}(x, x')$ can be obtained in a class of continuum-like causal sets, including those approximated by dS [27,36]. This makes it possible to explicitly calculate the causal set SSEE for the dS horizon.

An important aspect of the calculation of the EE is the introduction of a UV cutoff, which renders it finite. An unregulated quantum field in the continuum consists of infinitely many UV degrees of freedom which would yield an unbounded EE. When the regulated EE satisfies an area law, it is proportional to the spatial area of the entangled regions in units of the UV cutoff. This gives the scaling $S \propto a^{2-d}$ (for $d > 2$), where a is the UV cutoff in length dimensions and d is the spacetime dimension.⁵ This is also true in the case of quantum theories with local interactions [38].

⁴It is possible for example to have finite N corrections to this formula, which vanish in the continuum limit.

⁵For a heuristic argument for why the EE will in general be proportional to the spatial area of the entangling surface in units of the UV cutoff see [37].

The causal set provides a natural cutoff length scale $a = \rho^{-1/d} \propto N^{-1/d}$. Based on this, the expected UV-dependence of the entanglement entropy S of a scalar field in various dimensions is as shown in the table below, with (10) and (11) being special cases. Since the leading area term in $d = 2$ is a constant (as the spatial boundary of the entangling region is one or two points), one also considers the subleading contribution $c_1 \ln a$, where c_1 is a universal constant.⁶

Spacetime Dimension	$S(a)$	$S(N)$
$d = 2$	$c_1 \ln a + \text{const}$	$-c_1 \ln \sqrt{N} + \text{const}$
$d = 3$	$1/a$	$N^{1/3}$
$d = 4$	$1/a^2$	\sqrt{N}

Table 1: The dependence of the entropy S on the UV length cutoff a and causal set size N .

If instead $S(N) \sim N$, this means that S satisfies a spacetime *volume* rather than an area law. Interestingly, we will see that this is what commonly happens in the causal set when we compute the SSEE without any truncations.

2.3 Review of Causal Set SSEE for Nested Causal Diamonds in \mathbb{M}^2

In order to set the stage we review the results of [24] for causal sets approximated by the nested causal diamonds $\mathbb{D}_\ell^2 \subset \mathbb{D}_L^2 \subset \mathbb{M}^2$, with side lengths $2L > 2\ell$ (see Figures 1 and 3). In this special case, one can make comparisons with the continuum results of [21] which made use of the fact that the continuum SJ modes for \mathbb{D}_L^2 are explicitly known [26]:

$$\begin{aligned} f_k(u, v) &= e^{iku} - e^{ikv} \quad | \quad k = \frac{n\pi}{L}, \quad n \in \mathbb{Z}^\pm \\ g_k(u, v) &= e^{iku} + e^{ikv} - 2 \cos kL \quad | \quad k \in \ker(\tan(kL) - 2kL) \\ &\xrightarrow{m \rightarrow \infty} \left(m - \frac{1}{2}\right) \frac{\pi}{L} \approx \frac{m\pi}{L}, \quad m \in \mathbb{Z}^\pm. \end{aligned}$$

In the UV limit, i.e., for large k , the SJ spectrum takes the simple form $\lambda_k = \frac{L}{k}$ for both sets of modes. In this limit, these modes moreover become linear combinations of the same plane waves, but are out of phase. Thus the UV part of the SJ spectrum for both modes can be characterised by an integer n , with $k = \frac{n\pi}{L}$.

For a causal set approximated by \mathbb{D}_L^2 , the SJ spectrum was calculated using the $d = 2$ causal set retarded Green function (see Appendix B) [24]. Figure 2 shows a comparison of the continuum and causal set SJ spectra for \mathbb{D}_L^2 which match up to the characteristic “knee” mentioned in the Introduction. As the sprinkling density $\rho = N/V$ increases, the knee in the causal set SJ spectrum occurs at larger k values.

The continuum SSEE was calculated in [21] for $\mathbb{D}_\ell^2 \subset \mathbb{D}_L^2$ using a cutoff $a = 1/k_{\max}$ and shown to satisfy the expected “area” law of (5). However, the analogous calculation in the causal set, yielded a volume law, $S^{(c)} \propto N$, rather than an area law [24].

This surprising feature, which is markedly different from the continuum result, can be traced to the shape of the causal set SJ spectrum. As evident in Figure 2, beyond the

⁶When the spatial boundary is a single point $c_1 = -1/6$, and when it is two points $c_1 = -1/3$.

knee the causal set SJ spectrum contains a large number of near zero eigenvalues, which are absent in the continuum. In the causal set SSEE, (12), the generalised eigenvector v is required to lie outside the kernel of Δ_{C_O} . However, because of the nature of the causal set discretisation, fluctuations near the cutoff scale ρ^{-1} can yield eigenvectors that are “almost” but not strictly in the kernel. This is true in general of the discrete-continuum correspondence: as one gets closer to the spacetime discreteness scale ρ^{-1} , the relative fluctuations get larger. Thus, it is reasonable to expect that at such scales, the causal set SJ spectrum will deviate significantly from the continuum.

Indeed, as shown in [24], truncating the SJ spectrum of both $i\Delta_C$ as well as $i\Delta_{C_O}$ around this knee has the effect of giving back the expected $d = 2$ “area law” as in the continuum. Such a truncation can be motivated by appealing to the fact that the SJ modes f_k, g_k are combinations of plane wave modes with wavenumber $k = \frac{2\pi}{\nu}$, where ν is the wavelength. The causal set discreteness then gives a natural choice for the minimum wavelength $\nu_{\min} \sim \rho^{-1/2} = 2L/\sqrt{N}$. Since $k \sim \frac{n\pi}{L}$ for large k , this suggests a truncation to retain as many modes as $n_{\max} \sim \sqrt{N}$. The dimensionless causal set SJ eigenvalue λ^{cs} is related to the dimensionful continuum SJ eigenvalue λ by $\lambda^{cs} = \rho^{\frac{2}{d}}\lambda$. This means that $\lambda_{\min} = \frac{L^2}{\pi n_{\max}}$ corresponds to $\lambda_{\min}^{cs} \sim \frac{\sqrt{N}}{4\pi}$ when we truncate the SJ spectrum with $n_{\max} \sim \sqrt{N}$.

The choice of \sqrt{N} modes can also be justified by appealing to another aspect of the continuum picture. In the conventional spatial way of understanding a quantum field and its EE, the field is quantised on a spatial Cauchy hypersurface and the contributions to the EE come from the field modes on that Cauchy hypersurface. In the continuum we do not expect to have *more* field modes contribute to the SSEE than in the spatial case, when we are working with domains of dependence. While the space of our solutions $\dim(\Delta) = N$ is larger, the space of independent solutions given by the $\text{Im}(i\Delta)$ should remain the same as in the spatial picture. We expect the latter to be given in terms of the spatial volume (here the length) of the Cauchy hypersurface, so that the number of non-redundant solutions $\sim \sqrt{N}$ (where we have singled out the time-symmetric $t = 0$ diameter of the causal diamond). Alternatively, since λ has a dimension of $(\text{length})^2$, we may assume that it is more generally the product of an IR scale and a UV scale, $\lambda_{\min}^{cs} \sim \rho^{\frac{1}{2}}L \sim \sqrt{N}$. We note that since the number of the eigenvalues is $\sim N$, the reduction to \sqrt{N} modes is a very non-trivial restriction.

Thus, we have a *number truncation* characterised by n_{\max} which gives the number of (largest in magnitude) eigenvalues that are retained, or alternatively, a *magnitude truncation* λ_{\min}^{cs} which gives the minimum magnitude of the eigenvalues that are retained. These are related in \mathbb{D}_L^2 by

$$\lambda_{\min}^{cs} = \frac{N}{4\pi n_{\max}}, \quad (13)$$

but this relation may not hold more generally.

Once the truncation scheme is decided, the truncation needs to be implemented *twice*. This is the *double truncation* followed in [24] which we describe in some detail below for the specific case of $\mathbb{D}_{\ell}^2 \subset \mathbb{D}_L^2$. Our notation is a little heavy for the sake of clarity, but we will shed it for simpler notation subsequently.

The first truncation $n_{\max} \sim \sqrt{N}$ or $\lambda_{\min}^{cs} \sim \frac{\sqrt{N}}{4\pi}$ is on the SJ spectrum in \mathbb{D}_L^2 , which

therefore also truncates the operator $i\Delta_L^t$ and therefore the SJ Wightman function W_L to W_L^t . After the first truncation the region beyond the knee in the SJ spectrum of $i\Delta_L$ is removed, leaving behind a residual power law behaviour. Next, when $i\Delta_L^t$ is restricted to \mathbb{D}_ℓ^2 , i.e., $i\Delta_\ell^t(x, x') \equiv i\Delta_L^t(x, x')|_\ell$ the knee reappears once again in the spectrum of the corresponding integral operator $i\Delta_\ell^t$ in \mathbb{D}_ℓ^2 . Hence a second truncation with $n_{\max}^\ell \sim \sqrt{N_\ell}$ is necessary in the spectrum of $i\Delta_\ell^t$, which we denote by $i\Delta_\ell^{tt}$. Finally, the restriction $W_l^t \equiv W_L^t|_\ell$ of W_L^t to \mathbb{D}_ℓ^2 , must then be further projected onto this smaller (double) truncated subspace of the eigenbasis of $i\Delta_\ell^t$, to give us W_l^{tt} . Note that $i\Delta_\ell^{tt}$ is *not* the operator obtained after truncating the spectrum of the Pauli-Jordon operator $i\Delta_\ell$ in \mathbb{D}_ℓ^2 .

The reappearance of the knee in the spectrum of $\text{Im}(i\Delta_\ell^t)$ can be traced to the fact that the Pauli-Jordan integral operators $i\hat{\Delta}_L$ and $i\hat{\Delta}_\ell$ are defined over different integral domains and hence the spectrum of $i\hat{\Delta}_\ell$ cannot be obtained from a restriction of that of $i\hat{\Delta}_L$. This “non-locality” is an important feature of the SJ vacuum. Most importantly, without this second truncation, the full set of “near zero” elements in $\text{Im}(i\Delta_\ell^t)$ is not removed and this gives rise to a too-large SSEE.

This gives us a template for implementing the double truncation procedure more generally, for any $C_O \subset C$. Thus, the first truncation is performed on the SJ spectrum of $i\hat{\Delta}_C$ to give the truncated operator $i\hat{\Delta}_C^t$, and its associated Wightman function $W_C^t(x, x')$. The restriction of the truncated Pauli-Jordan function $i\Delta_{C_O}^t(x, x') = i\Delta_C^t(x, x')|_{C_O}$ corresponds to an operator $i\hat{\Delta}_{C_O}^t$ in C_O , i.e., for $x \in C_O$, $i\hat{\Delta}_{C_O}^t \circ v(x) = i \sum_{x' \in C_O} \Delta_{C_O}^t(x, x') v(x')$.

The second truncation is then performed on the spectrum of $i\hat{\Delta}_{C_O}^t$, which yields the operator $i\hat{\Delta}_{C_O}^{tt}$, as well as the projection $W_{C_O}^{tt}$ of the restriction $W_C^t(x, x')|_{C_O}$ to this second truncated eigenbasis. Thus the double truncated SSEE version of (12) is

$$\mathcal{S}^{(c)} = \sum_\mu \mu \ln |\mu|, \quad W_{C_O}^{tt} \circ v = i\mu \Delta_{C_O}^{tt} \circ v, \quad \Delta_{C_O}^{tt} \circ v \neq 0, \quad (14)$$

where tt denotes the double truncation procedure described above. We now drop the “ tt ” superscript for simplicity of notation, and refer to the spectrum as either truncated or untruncated.

2.4 Generalised Truncation Schemes

In what follows, we discuss ways in which to generalise the truncation procedure in \mathbb{D}_L^2 without explicit knowledge of the SJ spectrum in the continuum. Out of the several possibilities, the ones that would closely mimic the continuum would be those that satisfy an area law relation for the SSEE compatible with the Bekenstein-Hawking entropy, as well as complementarity.

We consider causal sets obtained by sprinkling into the finite volume “slab” between $[-h, h]$ in dS. As discussed in Section 2.1, the south and north Rindler-like wedges \mathcal{R}_{o_S} and \mathcal{R}_{o_N} are complementary to each other, and intersect only at the equator of the $t = 0$ 3-sphere. In the dS slab, these regions have hyper-hexagonal boundaries (see Figure 4). Both \mathcal{R}_{o_S} and \mathcal{R}_{o_N} are also time-symmetric and are the domains of dependence of time-symmetric $t = 0$ Cauchy slices, which are the Southern and Northern hemispheres of the 3-sphere, respectively.

Since the SJ spectrum of the hyper-hexagon is not known, we cannot resort to comparisons with the continuum as in the nested diamonds. In the course of our investigations we tried a very large number of different truncation schemes. Of these we focus on two particular schemes which we think are physically motivated and simple to generalise and moreover, give an SSEE which satisfies an area law.

The first choice we make is an estimation of the number truncation n_{\max} , inspired by the nested $d = 2$ diamonds, where $n_{\max} = \sqrt{N}$ for each of the two sets of modes. This was motivated by the fact that the number of modes should be proportional to the spatial volume of a Cauchy hypersurface. A natural generalisation of this is

$$n_{\max} = \alpha N^{\frac{d-1}{d}}. \quad (15)$$

Note that the identification of the spatial volume is neither uniquely nor covariantly defined, and hence there is no unique choice of α ; in particular one can deform the Cauchy hypersurface to one that has arbitrarily small spatial volume. In our investigations of the nested causal diamonds in \mathbb{M}^4 (Section C) we experimented with several values of α , including that corresponding to the volume of the time symmetric slice. In the de Sitter case, this latter factor turns out to be too large, leading to too small a truncation. As a result, we focus here only on values of α which give the most reasonable results, i.e., $\alpha = 1, 2$.

Our second choice is a new truncation scheme, which we dub the linear scheme. Since the SJ spectrum in the causal set is a power law and therefore linear in the log-log plot, up to a characteristic knee, it is reasonable to truncate the spectrum at the point where this linear regime ends. This requires an estimation of the end of the linear regime in the log-log plot. One method is to use the change in the slope of the logarithms of the data. We implement this in the following way: First, the logarithms of each n^{th} eigenvalue are taken along with the logarithm of its label n . Then the slope of the line between each nearest neighbor pair⁷ of data points is computed. Due to fluctuations in the causal set data, these slopes also fluctuate when going from one pair's slope to the next, even in the (approximate) power law regime. In order to smooth out these fluctuations, the slopes are binned and averaged. Then, a smooth interpolating function is fit to the averaged slopes as shown in Figure 5. This interpolating function can then be used to track the drop in the slope and set the truncation number or magnitude. The region of nearly constant (negative) slope m is first identified, and the estimation of the knee corresponds to a drop to a more negative m' . A choice is then made of the fractional drop $\delta = \frac{m-m'}{m}$ to obtain the knee. We take the magnitude of the eigenvalue at this estimated knee as our magnitude truncation, or the number n_{\max} (rounded to the nearest integer) at which this happens as our number truncation. We have explored various choices of δ , also allowing it to be different in the slab and in the Rindler-like wedge.

An advantage of the linear truncation over the generalised number truncation (15) is that it is covariantly defined, without appealing to any features of a Cauchy surface and the associated ambiguity of choosing a proportionality constant. There is of course the fine tuning that comes with the choice of δ and the hope is to be able to find a suitable range of values, as much as the quality of data allows.

⁷An alternative method, which yields similar results, is to take the slopes of more than a pair (say, every 50) of nearest eigenvalues.

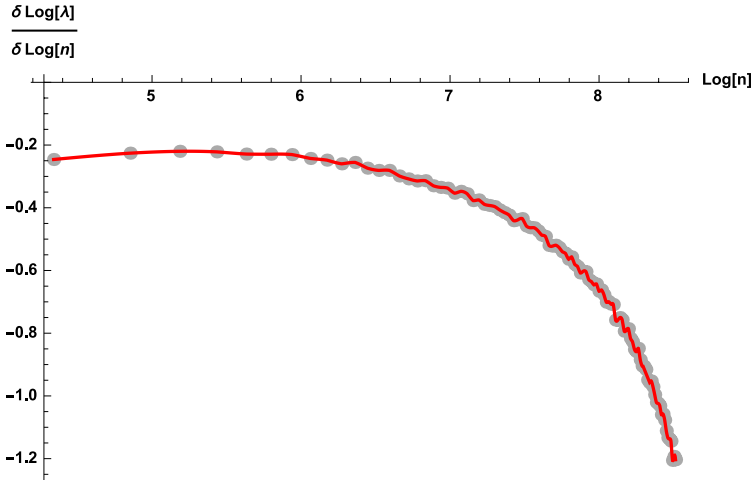


Figure 5: Slopes of the log-log SJ spectrum in dS_4 . Data points are binned averages and the curve is an interpolating function fit to the data.

In all the cases we study, the numerically generated causal set SJ spectrum can additionally be used to estimate the power law behaviour of λ^{cs} as a function of n . Rescaling the spectrum by $\rho^{-\frac{2}{d}}$ collapses the data in the linear regime, so that

$$\rho^{-2/d} \lambda^{cs} = \frac{b}{n^a}, \quad (16)$$

where the exponent a and the constant b can be determined empirically. For \mathbb{D}_L^2 , for example, $a = 1$ and $b = 1/(4\pi)$. For the dS_2 , dS_4 slabs and associated Rindler-like wedges these values are given in the following table, where the slab height has been chosen to be $h = 1.2$.

Spacetime	Slab	Wedge
dS_2	$a \sim 1, b \sim 1.68$	$a \sim 1, b \sim 0.26$
dS_4	$a \sim 0.25, b \sim 2.16$	$a \sim 0.36, b \sim 0.78$

Table 2: The values of parameters a and b in (16) determined from the spectrum of $i\Delta$ in the regions considered.

This also allows us to translate n_{\max} (picked either by the number or linear truncation method) into a magnitude truncation λ_{\min}^{cs} for this choice of h . We have not however studied the effect of varying h on the parameters a and b and whether or not the spectrum can be collapsed to a universal form.

3 Results

The simulations presented here were performed using Mathematica on an HP Z-8 workstation with 320GB pooled RAM. For larger N values, a significant fraction of this pooled memory was used in the simulation, when all the trials for fixed N are parallelised. The

results presented here are the culmination of extensive exploration of various truncation schemes, including certain magnitude truncations not described in Section 2.4. Here we only present results from the two described in Section 2.4 and for choices of α and δ which best satisfy the criterion of an area law compatible with the Bekenstein-Hawking entropy. As mentioned in Section 2.4, the two Rindler-like wedges are identical and hence complementarity should be automatically satisfied. In our investigations, we also calculated the SSEE for a causal diamond in the slab spacetime, whose complement is not necessarily a causal diamond, but for this work we present results only from the Rindler-like wedges, since these are of most interest for the dS horizons.

3.1 dS₂

In dS₂, the two complementary regions \mathcal{R}_{o_S} and \mathcal{R}_{o_N} are each conformal to causal diamonds. The simulation results we present are for a slab of dS₂ of height $h = 1.2$ into which we sprinkle causal sets with sizes $\langle N \rangle$ ranging from 2000 to 16000.

Figure 6 shows the dependence of the SSEE with N without truncating the SJ spectrum. The SSEE clearly scales linearly with N and therefore obeys a spacetime volume law, as in the case of the $d = 2$ nested diamonds [24].

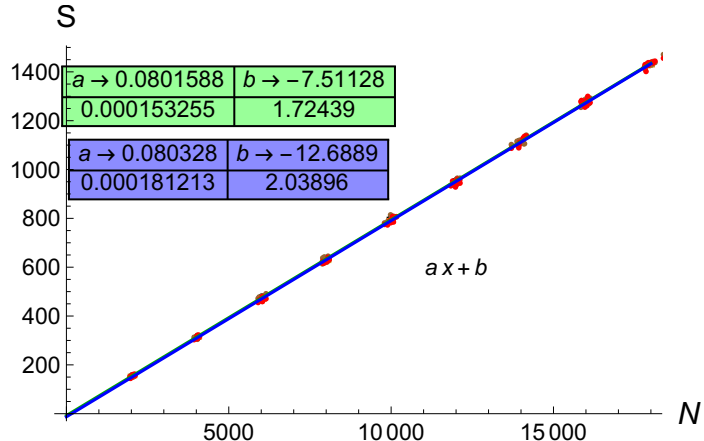


Figure 6: Untruncated SSEE vs. N in the dS₂ slab of height $h = 1.2$ for the two Rindler-like wedges \mathcal{R}_{o_S} and \mathcal{R}_{o_N} (shown in green and blue). The best fits are shown.

Next we implement the truncation schemes discussed in Section 2.4 for the SJ spectrum for a causal region of cardinality N_s . For each $\langle N \rangle$, we run 10 simulations for the number truncation while we run 5 simulations for the linear truncation. For the latter, the estimation of the linear regime is done for the SJ spectrum in the slab as well as for the SJ spectrum in the Rindler-like wedges.

For the number truncation (15) we work with α values of 1 and 2, the latter being the analogue of the 2d causal diamond truncation.⁸ For the linear truncation scheme, different

⁸Note that while n_{\max} in our review of the 2d causal diamond denoted the maximum number of modes of each family of f and g eigenfunctions, here we refer to it as the total number of eigenfunctions irrespective of degeneracies. Hence the two-fold degeneracy of the 2d diamond amounts to keeping a total of $2\sqrt{N}$ eigenvalues in the terminology henceforth.

values of δ were explored. We found that the one most compatible with the area law is $\delta \sim 0.1$ in both the slab and the Rindler-like wedge.

In Figure 7a we show the log-log plot of the untruncated causal set SJ spectrum of the dS₂ slab, with these three choices for truncation marked. All three clearly lie in the linear regime, with the linear truncation being the closest to the knee. In Figure 7b we show the log-log spectrum of the generalised eigenvalue equation before and after truncation. What is striking is the drastic reduction in not only the number but also the magnitude of the eigenvalues. It is this feature that seems to make it possible to recover an area law after truncation.

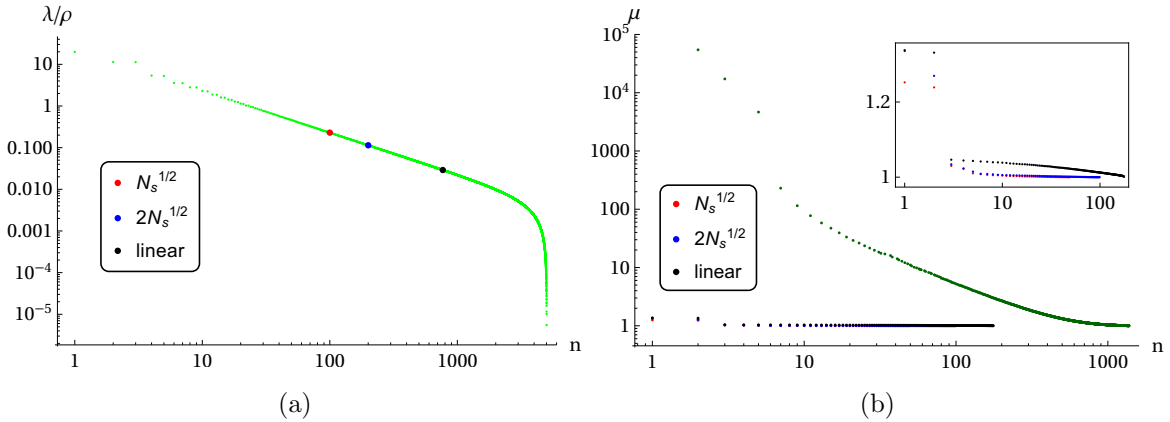


Figure 7: (a) The SJ spectrum for an $N = 10^4$ causal set sprinkled into the dS₂ slab. Three different truncations choices are marked. (b) The spectrum for the SSEE (12) with and without these truncations.

Finally, in Figure 8 we show the SSEE calculated using the above three truncations for both \mathcal{R}_{oS} and \mathcal{R}_{oN} . For each truncation, on the left we show the fit to the logarithmic behaviour

$$\mathcal{S}^{(c)} = a \ln N + b, \quad (17)$$

(where the expected value of a is $1/6$) and on the right, the fit to the volume behaviour $aN + b$. The errors in the best fit parameters are given below these values. The fit and corresponding uncertainties are found using the least square method. We see in all three cases that the data has a high degree of scatter, which is also the case for the $d = 2$ nested diamonds [24] and seems to be a characteristic of $d = 2$. All cases are reasonably consistent with an area law, but the linear truncation is surprisingly more consistent with a volume law. All cases also satisfy complementarity up to Poisson fluctuations.

From these results we conclude that the truncation that is closest to the expected EE values is the choice $n_{\max} = 2\sqrt{N}$, with a and b values given in Figure 8b. This case gives $a \sim 0.18$ which is closest to the expected value of $1/6$.

3.2 dS₄

The dS₄ slab is again taken to have height $h = 1.2$. We consider causal set sprinklings with $\langle N \rangle$ ranging from 2000 to 16000.

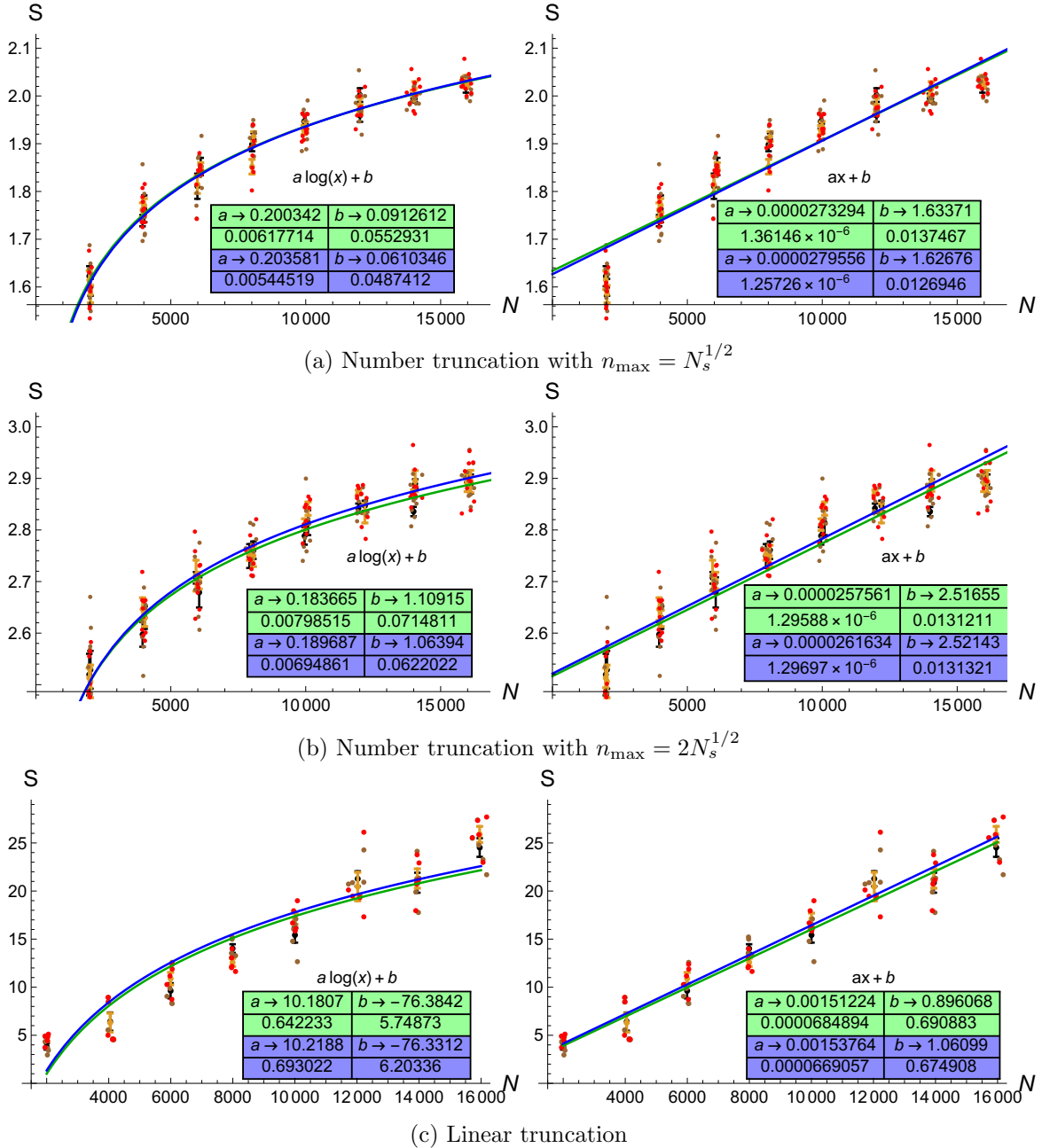


Figure 8: SSEE vs. N with three different choices of truncation in dS_2 . The green and blue represent the data for the two Rindler-like wedges. A comparison of the two fits $a \ln x + b$ and $ax + b$ is shown on the left and the right for each choice of truncation.

In Figure 9 we show the untruncated SSEE which again clearly scales linearly with N and therefore obeys a spacetime volume law.

We present results for three choices of truncations, the number truncations $n_{\max} = N^{\frac{3}{4}}$, $2N^{\frac{3}{4}}$ and the linear truncation. We run 10 simulations for each fixed $\langle N \rangle$ for both

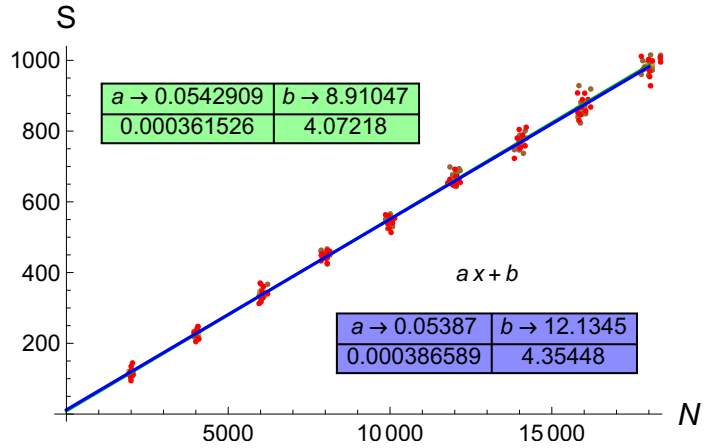


Figure 9: Untruncated SSEE vs. N in a dS_4 slab of height $h = 1.2$ for the two Rindler-like wedges \mathcal{R}_{oS} and \mathcal{R}_{oN} (shown in green and blue). The best fits are shown.

types of truncation. As in dS_2 , for the latter, the estimation of the linear regime is done for the SJ spectrum in the slab as well as for the SJ spectrum in the Rindler-like wedges. We find that a choice of $\delta \simeq 0.15$ for both the slab and the Rindler-like wedge spectrum gives the best results. Note that since the knee is fairly sharp in the log-log spectrum, even a seemingly large tolerance does not lead to very drastic changes in the spectrum but does change the SSEE so obtained.

In Figure 10a we show the causal set SJ spectrum in the dS_4 slab with the different truncations marked, and in Figure 10b we show the generalised spectrum with and without these truncations. Again the broad features are the same – the truncations lie in the linear regime of the SJ spectrum and drastically cut down both the magnitude and number of the generalised spectrum. However, the differences in the generalised spectrum post truncation are more marked in $d = 4$.

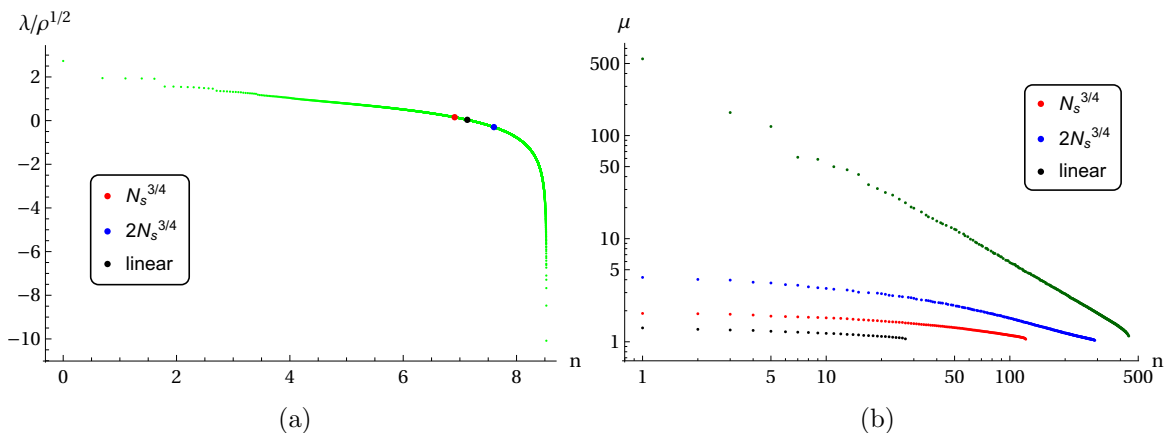


Figure 10: For $N = 10k$ in dS_4 , (a) is the spectrum of $i\Delta$ with different truncations marked, and (b) is a plot of the solutions of the generalised equation (12) for these truncations.

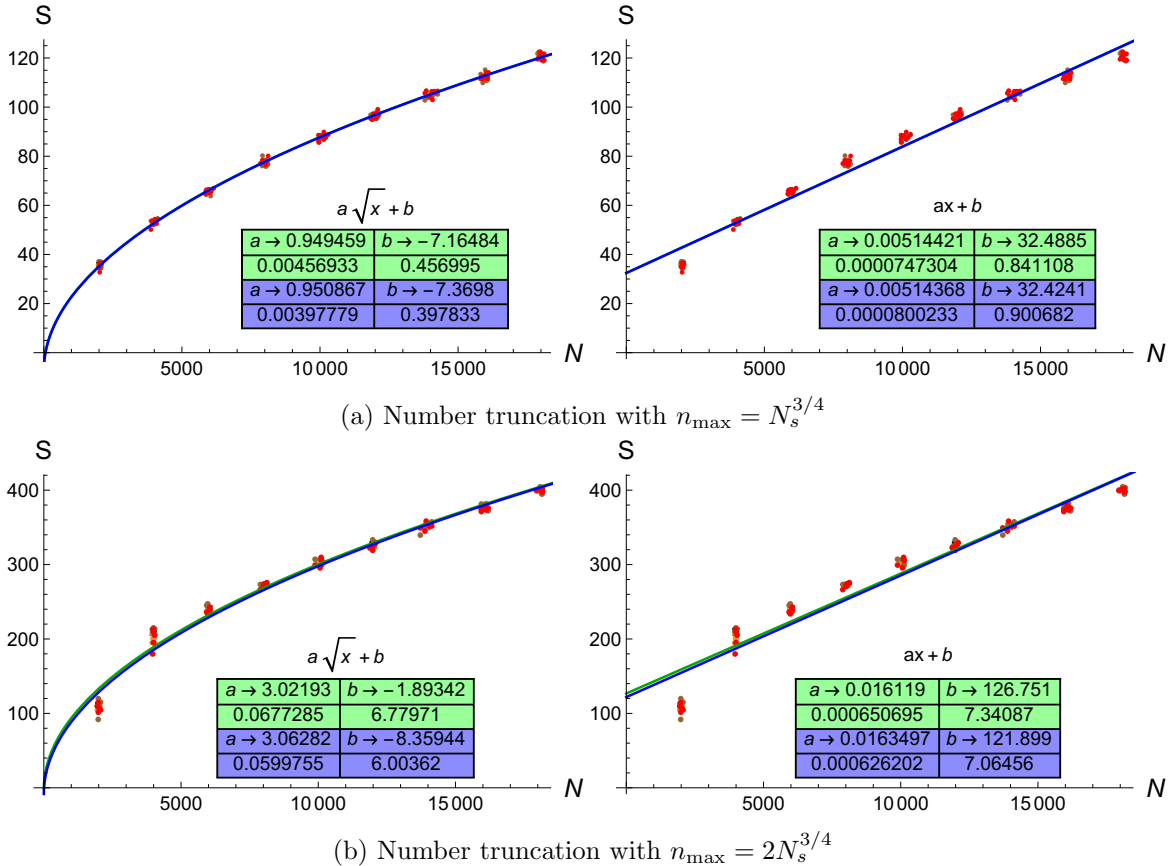
The area law for the SSEE for dS_4 is given by

$$S = a\sqrt{N} + b. \quad (18)$$

With $h = 1.2$, we expect $a \sim 0.17$ for the Bekenstein-Hawking entropy for the dS horizon (10). In Figure 11 we show the results for the SSEE. We note that interestingly, the scatter is far less than in $d = 2$, which makes the results easier to interpret.

In all cases we see that an area law and complementarity are compatible with the data, but that the linear truncation scheme is also compatible with a volume law. The number truncations $n_{\max} = N^{3/4}$, and $n_{\max} = 2N^{3/4}$ give a much more convincing area law.

A comparison with the Bekenstein-Hawking formula however shows that *all* the values of a in Figure 11a exceed the expected value of $a = 0.17$. So even though an area law is obtained, it is one that contains more entropy than expected. For $n_{\max} = N^{3/4}$ the SSEE is about 5 times larger, and the difference is even greater for $n_{\max} = 2N^{3/4}$. Perhaps this is not surprising because we do not know the proportionality constant α in (15), although it is reasonable to expect an α of order 1. The linear truncation gives an SSEE that is closer to the Bekenstein-Hawking entropy, although it again is in excess.



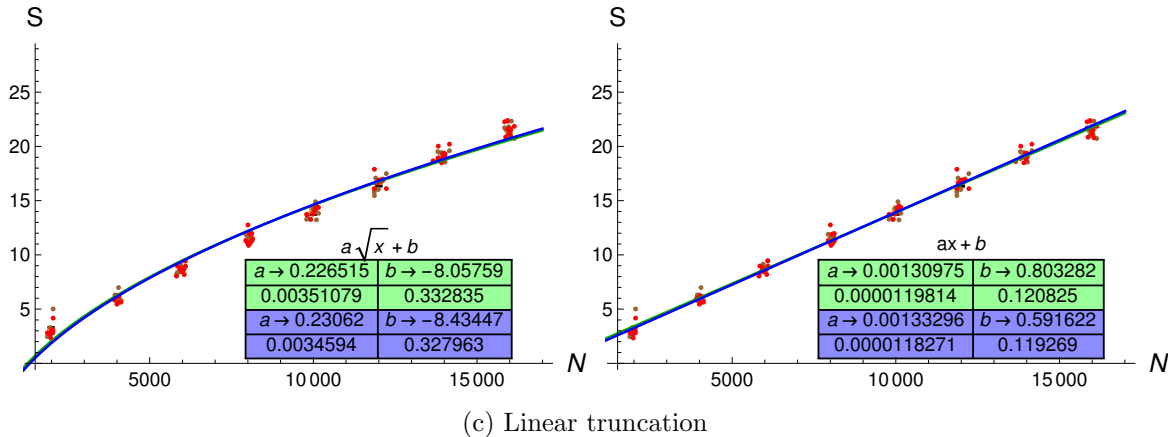


Figure 11: SSEE vs. N with different choices of truncation in dS_4 . The green and blue represent the data for the two Rindler-like wedges. A comparison of the two fits $a\sqrt{x} + b$ and $ax + b$ is shown on the left and the right for each choice of truncation.

4 Discussion

Numerical studies such as the one we have carried out in this paper have shown that an excess SSEE due to the small eigenvalues of the SJ spectrum is a common occurrence, and thus generically gives rise to a volume rather than an area law. In this work we have presented evidence that the causal set SSEE for $dS_{2,4}$ horizons satisfies a volume rather than an area law, when the full causal set SJ spectrum is used.

On implementing certain double truncation schemes on the SJ spectrum, inspired by the \mathbb{D}_L^2 case, we show that area laws can be obtained, which also, as expected, satisfy complementarity. In this sense, the properties of the causal set SSEE obtained in [24] for the nested causal diamonds $\mathbb{D}_\ell^2 \subset \mathbb{D}_L^2$ appear to be universal.

Out of the many truncation schemes explored in dS_2 , the number truncation $n_{\max} = 2\sqrt{N}$ gave results most compatible with the Bekenstein-Hawking entropy, while for dS_4 , the linear truncation gave the best results. In both cases, the area law is satisfied up to the expected order of magnitude. There is a small over-estimation of the EE compared to the BHE in both cases, but we cannot attribute any physical significance to it since the exact value of the EE depends not only on the choice of truncation scheme but also on the parameters α and δ . For now it suffices that there are choices of these parameters which give us the correct order of magnitude estimate for the area law.

In our investigations, several choices of these parameters have been scanned, with the values exhibited here being the most optimal in terms of the area law and data compatible with complementarity. While the possibility always exists of further fine-tuning, or using a different truncation scheme, this is not necessarily helpful without further physical understanding. One might of course also resort to the possibility that N is not large enough and what we are seeing are finite size effects. We thus view our present study as only the start of a more systematic *analytic* understanding of the nature of the causal set SSEE in curved spacetimes.

There are several distinctive features of the dS EE calculation which we now summarise.

To begin with, the SSEE (12) does not specify a choice of vacuum. However, the SJ vacuum prescription is the only way we know how to define a vacuum in the causal set (in the continuum it is a uniquely defined vacuum in a finite spacetime region) and hence this is the choice we make. Importantly, the causal set dS SJ vacuum is distinct from the known Mottola-Allen vacua in the continuum as shown in [28]. Thus, if we are to take the causal set as more fundamental than the continuum, this suggests that the “correct” QFT vacuum for calculating the SSEE is not one of the Mottola-Allen vacua, but rather one with modified UV properties.

The truncation procedure, while essential for an area law, remains poorly understood. The fact that the SSEE obeys a volume law without truncation seems to arise from the non-locality of the causal set. As discussed in [38] systems with long-range order exhibit volume rather than area laws. The non-locality in a causal set, which enables an element near the past boundary to be linked to one near the future boundary, is fundamental to the discrete-continuum correspondence. Localising influences near sets of measure zero, even if they are genuine horizons, is not commensurate with this feature. Thus, a volume law seems particularly convincing in causal set theory. However, the lack of complementarity due to a volume law could also mean that the entanglement entropy is not bipartite, or that the entropy we are computing is dominated not by the entanglement entropy but by some other form of entropy (like the entropy of coarse graining). These issues need to be investigated further. Since area laws are a fundamental feature of General Relativity, which causal set theory must approximate, locality must be emergent, and with it, an area law for the SSEE.

Truncation also throws up new problems, namely the possibility of causality violation, as for example in the nested causal diamonds in M^2 . Here, the condition $i\Delta(x, x') = 0$ for spacelike separated points x and x' does not always hold for the truncated $i\Delta$. It can be shown that this acausality averages to zero over multiple sprinklings, but this nevertheless points to the need for a deeper understanding of the truncation process.

A possible way in which truncation may be avoided is to note that there could be significant deviations from manifold-likeness in the causal set at smaller scales. The correct UV completion of spacetime is likely not manifold-like at all and could significantly change the SJ spectrum and in turn the SSEE. This conjectured UV completion may be the missing ingredient in our discussion, but we are far from an understanding of what this might be.

As we have seen and as shown in [24], while the causal set offers a ready covariant spacetime cutoff, the recovery of an area law for the SSEE in dS, though possible, is not straightforward. Suggestions in [25] for a deeper understanding from an Algebraic Quantum Field Theory perspective need to be explored further. Recently the continuum dS SJ spectrum in the slab has been found analytically [29], and offers us a possible route to calculating the continuum dS SSEE, and hence finding a more physically motivated truncation. Future work in this direction should hopefully shed some light on the questions that we have raised in this work.

Acknowledgements: We thank Fay Dowker for helpful discussions. YY acknowledges financial support from Imperial College London through an Imperial College Research Fellowship grant, as well as support from the Avadh Bhatia Fellowship at the University of Alberta. SS is supported in part by a Visiting Fellowship at the Perimeter Institute. Re-

search at Perimeter Institute is supported in part by the Government of Canada through the Department of Innovation, Science and Economic Development Canada and by the Province of Ontario through the Ministry of Colleges and Universities.

Appendix A Causal Sets and Sprinkling

Causal sets are proposed discrete underpinnings of spacetime. They are partially ordered sets consisting of a set of spacetime elements and the ordering relation among them. The causal set elements $x \in \mathcal{C}$ and their ordering relation (which is the causal precedence relation \preceq) satisfy a number of conditions: $\forall x \in \mathcal{C}, x \preceq x$ (reflexivity); $\forall x, y \in \mathcal{C}, x \preceq y \preceq x$ implies $x = y$ (antisymmetry); $\forall x, y, z \in \mathcal{C}, x \preceq y \preceq z \implies x \preceq z$ (transitivity); $\forall x, y \in \mathcal{C}, |I(x, y)| < \infty$, where $|\cdot|$ denotes cardinality and $I(x, y)$ is the causal interval defined by $I(x, y) := \{z \in \mathcal{C} | x \preceq z \preceq y\}$, (local finiteness).

Ultimately the causal set dynamics will dictate which causal sets are produced and how. At present this dynamics is a work in progress. Meanwhile a causal set can be produced through the process of sprinkling: randomly placing points in a Lorentzian manifold following a Poisson distribution. Sprinklings in dS are shown in Figure 12.

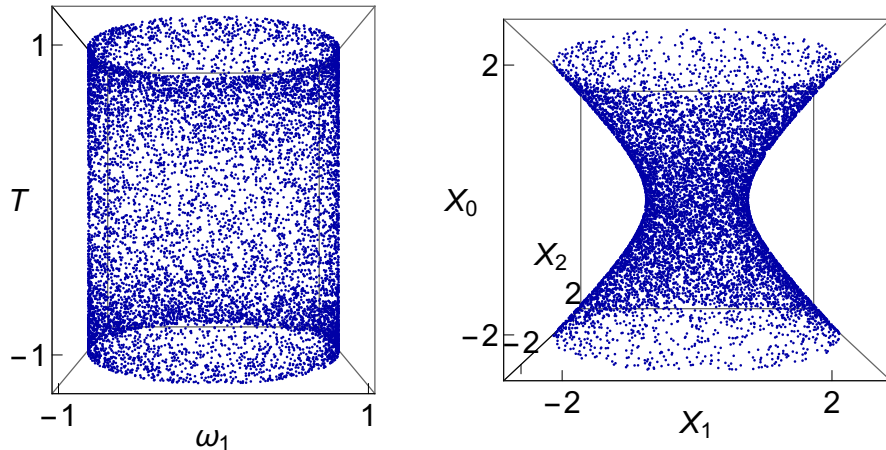


Figure 12: A sprinkling of $N = 10000$ elements into the metric of (4) for the time interval $-1.2 < T < 1.2$.

A common representation of a causal set is by a type of adjacency matrix called the causal matrix C . The causal matrix is defined as

$$C_{xy} = \begin{cases} 1 & \text{for } x \preceq y \\ 0 & \text{otherwise} \end{cases} \quad (19)$$

We have used the notation that the indices xy correspond to the matrix entry relating causal set elements x and y .

Another useful representation of a causal set is using the link matrix L . The link matrix

is defined as

$$L_{xy} = \begin{cases} 1 & \text{for } x \preceq^* y \\ 0 & \text{otherwise} \end{cases} \quad (20)$$

where we have introduced a link \preceq^* as a nearest neighbor relation such that $x \preceq y$ but with no $z \in C$ as an intermediate relation $x \preceq z \preceq y$. The link matrix L is also sometimes labelled as L_0 . The retarded Green functions discussed in the next appendix are expressed in terms of the causal and link matrices.

Appendix B The SJ Vacuum and Green Functions

Entanglement entropy is defined relative to a pure state. When a quantum field is in a pure state, its entropy of entanglement is zero. If the geometry in which the field resides is split into two complementary subregions, the quantum field's restriction to either subregion is no longer pure (it becomes mixed) and produces a non-zero EE. The pure state of SSEE is given by the Sorkin-Johnston (SJ) vacuum state, namely the SSEE vanishes when the quantum field is in the SJ state. We review the definition of the SJ vacuum state for a free scalar quantum field in this appendix. A key ingredient in the construction of this state is the retarded Green function. We also review the definition of this Green function in causal set theory.

The SJ prescription uses the Pauli-Jordan or spacetime commutator function

$$\begin{aligned} i\Delta(x, x') &= \langle 0 | [\phi(x), \phi(x')] | 0 \rangle \\ &= W(x, x') - W(x', x), \end{aligned} \quad (21)$$

where x and x' are points in *spacetime*, and W is the Wightman or two-point correlation function. $i\Delta$ is a c-number and (21) is therefore independent of the state in which it is computed. This is in contrast to W which is state dependent and in fact can be used to define the state. An alternative representation of Δ is the following one in terms of the retarded and advanced Green functions

$$\Delta(x, x') = G_R(x, x') - G_A(x, x'), \quad (22)$$

where G_R and G_A both satisfy $(\square - m^2)G_{R,A} = -\delta^d(x - x')/\sqrt{-g}$ and $G_A = G_R^T$.

In $d = 2$ and for any causal set approximated by flat or curved continuum geometries, the retarded Green function is

$$G_R^{(2)} = \frac{1}{2}C(\mathbb{I} - \frac{m^2}{2\rho}C)^{-1}, \quad (23)$$

where C is the causal matrix and \mathbb{I} is the identity matrix.

In $d = 4$, and for causal sets approximated by Minkowski spacetime or the dS case with coupling ξ , the retarded Green function is [27]

$$G_R^{(4)}(x, x') \equiv \sum_{k=0}^N a^{(k+1)} b^k L_k(x, x') = a L_0 (\mathbb{I} - b a L_0)^{-1}, \quad (24)$$

where $a = \frac{1}{2\pi} \sqrt{\frac{\rho}{6}}$, $b = -\frac{1}{\rho}(m^2 + (\xi - \frac{R}{6}))$, L_k is the product of the link matrix (20) with itself k many times, R is the scalar curvature, m the mass⁹, and N is the size of the causal set.

Since $i\Delta$ (or G_R , from which one obtains $i\Delta$ through (22)) is the starting point of the SJ prescription, this makes the prescription manifestly covariant. In a region of spacetime \mathcal{R} , $i\Delta$ defines an integral operator over the Hilbert space of square integrable functions $\mathcal{L}^2(\mathcal{R})$. Under suitable conditions (which are satisfied in finite-volume regions of spacetime such as the ones we consider in this paper) and in globally hyperbolic spacetimes (or subregions), $i\Delta$ is self-adjoint and can be decomposed into its positive and negative eigenspace.

Let u_k, v_k be the normalised positive and negative eigenfunctions of $i\Delta$ respectively, and $\pm\lambda_k$ their eigenvalues, such that

$$\int dV' i\Delta(x, x') u_k(x') = \lambda_k u_k(x), \quad (25)$$

$$\int dV' i\Delta(x, x') v_k(x') = -\lambda_k v_k(x), \quad (26)$$

where dV is the invariant volume element of the spacetime and $\lambda_k > 0$, then $i\Delta$ can be expressed in its eigenbasis as the expansion

$$i\Delta(x, x') = \sum_k \{\lambda_k u_k(x) u_k^\dagger(x') - \lambda_k v_k(x) v_k^\dagger(x')\}. \quad (27)$$

Finally, the SJ prescriptions is to define the SJ Wightman function W_{SJ} as a restriction of the expansion (27) to its positive part

$$W_{SJ}(x, x') \equiv \text{Pos}(i\Delta) = \sum_k \lambda_k u_k(x) u_k^\dagger(x'). \quad (28)$$

Every Wightman function defines a vacuum state, so the SJ Wightman function defines the SJ vacuum state of the theory. The field operator $\phi(x)$ in terms of these eigenfunctions is $\phi(x) = \sum_k \sqrt{\lambda_k} \{a_k u_k(x) + a_k^\dagger u_k^*(x)\}$, but we will not require the field and will only need to work directly with W in (1) or (12). Since we consider Gaussian theories, W contains all the information in the theory. For some studies of the SJ vacuum see [28, 40–42].

From its definition it is evident why the SJ state is a pure state for the SSEE. Since W_{SJ} is the positive eigendecomposition of $i\Delta$, the eigenvalues of W_{SJ} coincide with the positive eigenvalues of $i\Delta$. Therefore in (1), the solutions λ will be solely 1's and 0's. Upon inserting these in $\lambda \ln \lambda$ and summing them in (1) we get zero contribution to the entropy.¹⁰

The SJ vacua in many cases agree with conventional choices of vacua (for example in static spacetimes [43]) but are more general. In [28] the SJ vacua in dS were studied in detail. Among the cases that were studied were those that we consider in this paper. These include causal set discretisations of dS_{2,4} with a range of masses $m \geq 0$ for the free scalar field. In some cases, such as the massive theory in dS₂, the SJ vacuum coincided with other

⁹For a detailed discussion of the concept of mass in dS see [39].

¹⁰This is the case because both $0 \ln 0 = 0$ and $1 \ln 1 = 0$.

known vacua known as the Motolla-Allen α -vacua [44, 45]. In general, however, it was found that the vacua did not coincide with the continuum α -vacua. The causal set SJ vacuum in dS_4 for example, while de Sitter invariant, does not resemble any known vacua from the continuum. Also, interestingly, the causal set SJ vacuum is well-defined for all masses and couplings, including the minimally coupled massless case which is typically considered ill-defined [44, 46]. In this paper we use the SJ vacua found in [28] as our starting point, i.e., as the pure states of our SSEE. We use W_{SJ} in (12) and we use the causal set retarded Green function (24) to define $i\Delta$ in (12).

Appendix C Nested Causal Diamonds in \mathbb{M}^4

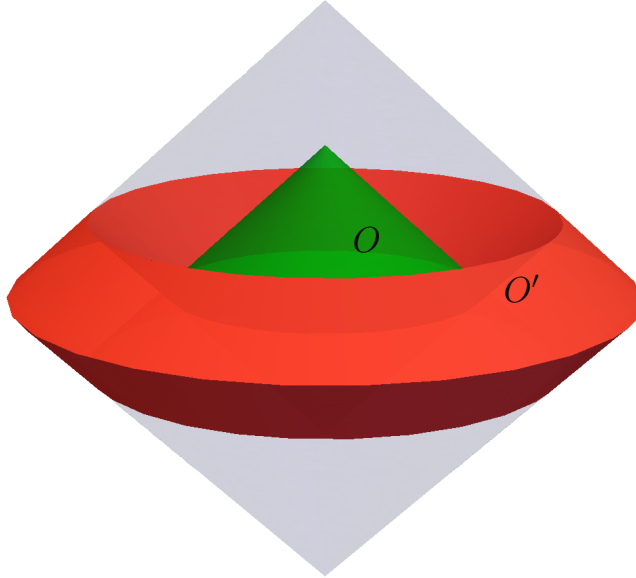


Figure 13: A nested causal diamond O and its complement O' in 3d.

Here we present some results for nested causal diamonds in \mathbb{M}^4 which is a non-trivial extension of the \mathbb{M}^2 case.

We consider a similar set up to \mathbb{M}^2 , namely nested causal diamonds $\mathbb{D}_\ell^4 \subset \mathbb{D}_L^4 \subset \mathbb{M}^4$. The causal complement $O' \subset \mathbb{D}_L^4$ of \mathbb{D}_ℓ^4 is connected and is the domain of dependence of a $d = 3$ open ball with a concentric spherical hole. We show this connectivity in Figure 13, where one of the dimensions has been suppressed.

In \mathbb{D}^4 , the entropy-area relation $S = A/4$ of (6) is

$$S = \pi r^2, \quad (29)$$

where r is the radius of the smaller diamond. The expression in the causal set, (9), is

$$S^{(c)} = \sqrt{\frac{3\pi}{2}}(r/R)^2\sqrt{N}, \quad (30)$$

where R is the radius of the larger diamond. In our simulations we set $r/R = 0.6$, therefore we expect $S \approx 0.78\sqrt{N}$.

We consider a number truncation with $n_{\max} = N^{3/4}$ in all regions, as well as a number truncation with $n_{\max} = N^{3/4}$ in \mathbb{D}_L^4 and \mathbb{D}_{ℓ}^4 while $n'_{\max} = 2N^{3/4}$ in the complement of \mathbb{D}_{ℓ}^4 . The motivation for the factor of 2 in the latter number truncation is that the relative spatial volume of the subset of the $t = 0$, time-symmetric Cauchy slice that lies in the complementary region is around twice as large as the subset that lies in \mathbb{D}_{ℓ}^4 . We also consider the linear truncation with $m' = -0.25 - |\epsilon|$ and $\epsilon = 0.05$ (or $\delta = 0.2$) in all regions.

In the simulations, we consider $\langle N \rangle$ values ranging from 4000 to 18000. For each $\langle N \rangle$ we consider 5 realisations.

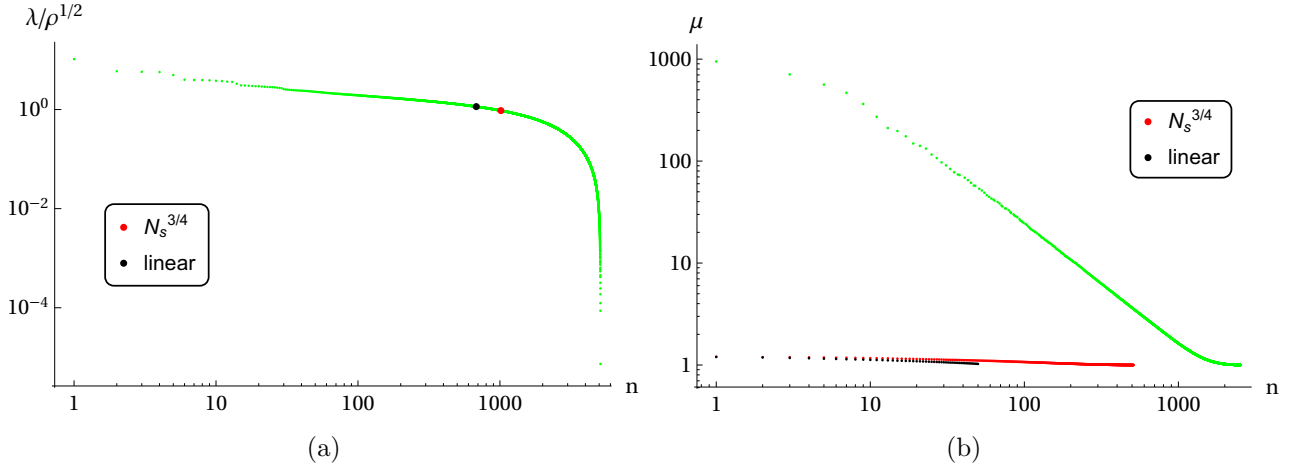


Figure 14: For $N = 10k$, (a) is the spectrum of $i\Delta$ with different truncations marked, and (b) is a plot of the solutions of the generalised equation (12) for these truncation schemes.

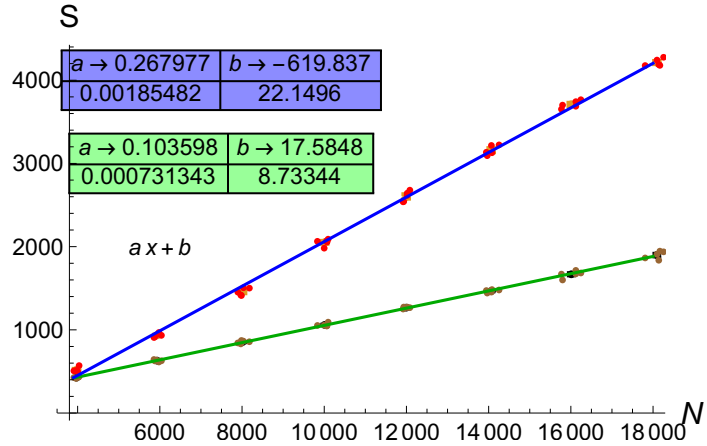


Figure 15: SSEE vs. N without truncation. Green represents the data for \mathbb{D}_{ℓ}^4 and blue represents its complementary region. The best fits are shown.

In Figure 14a we show the SJ spectrum for \mathbb{D}_L^4 , and where the truncations we consider

lie. We also show the SSEE eigenvalues μ in Figure 14b for one realisation. The causal set SSEE without truncation is shown in Figure 15 and can be seen to obey a spacetime volume law as anticipated.

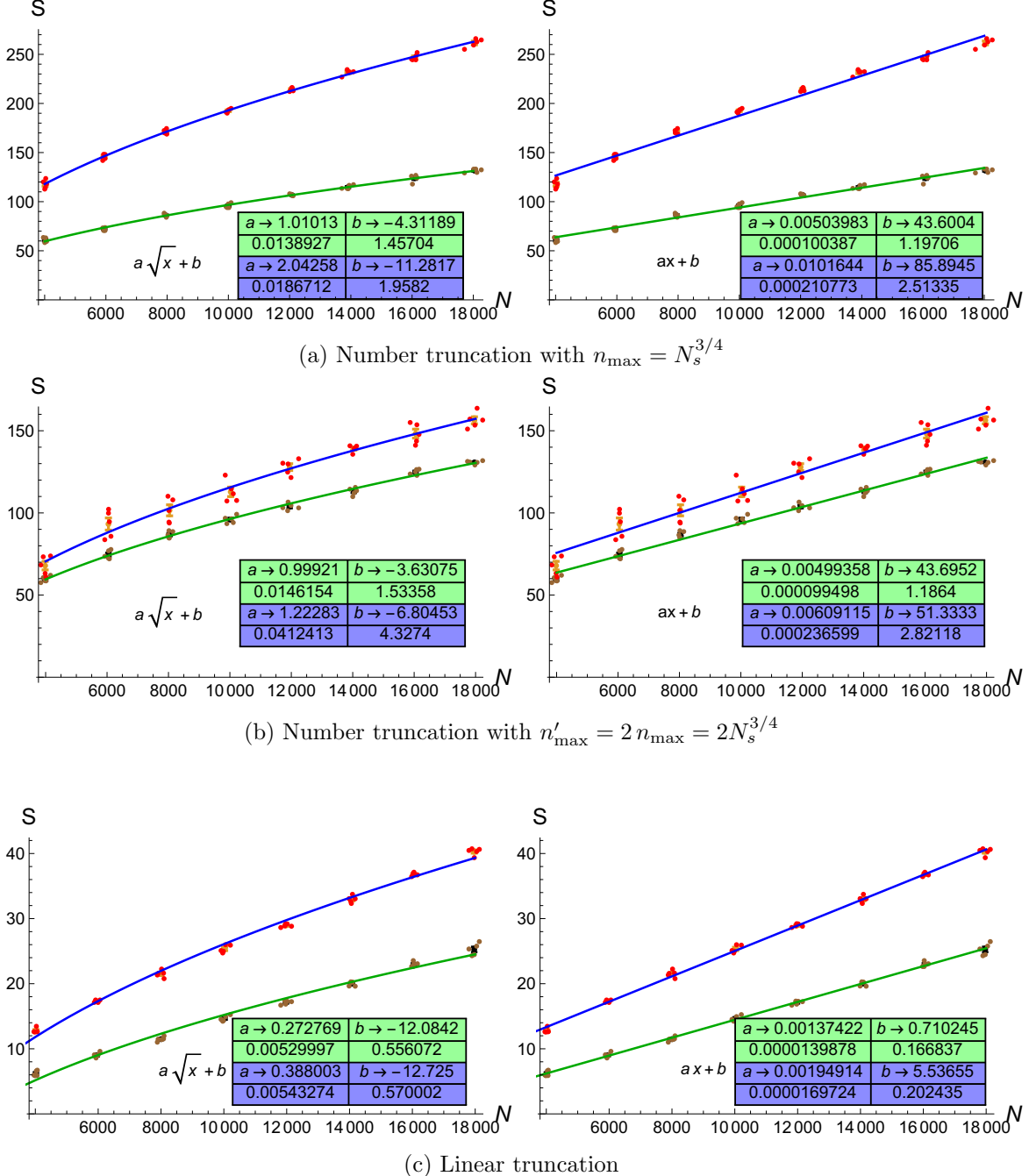


Figure 16: SSEE vs. N with different truncations. Green represents the data for \mathbb{D}_ℓ^4 and blue represents its complementary region. A comparison of the two fits $a\sqrt{x} + b$ and $ax + b$ is also shown. Here n'_{\max} is the number truncation in the region complementary to \mathbb{D}_ℓ^4 .

Next, we show in Figure 16 how the SSEE is modified with the application of the various truncations. An area law is recovered with the two number truncations $n_{\max} \propto N^{3/4}$, while the linear truncation is more consistent with a volume law. This is similar to what we found in the dS cases we studied above. The area law coefficients in most cases are ~ 1 and are therefore close to the expected value 0.78. What is more challenging and non-trivial here, compared to the dS cases, is achieving complementarity. The geometries of \mathbb{D}_{ℓ}^4 and its complement are very different (see Figure 13) and therefore the truncations ought to take this difference into account.

As we can see by comparing Figures 16a and 16b, it is correct to truncate the complementary region more than \mathbb{D}_{ℓ}^4 . The SSEE can get closer to satisfying both complementarity and the expected area law coefficient if one appropriately tunes the proportionality constant in $n_{\max} \propto N^{3/4}$. As discussed in the main text, we do not have a covariant argument by which to uniquely set this proportionality constant. In the absence of such an argument, we do not pursue tuning the constant(s).

References

- [1] J. D. Bekenstein, “Black holes and the second law,” *Lett. Nuovo Cim.*, vol. 4, pp. 737–740, 1972.
- [2] J. D. Bekenstein, “Black holes and entropy,” *Phys. Rev.*, vol. D7, pp. 2333–2346, 1973.
- [3] J. D. Bekenstein, “Generalized second law of thermodynamics in black hole physics,” *Phys. Rev.*, vol. D9, pp. 3292–3300, 1974.
- [4] G. W. Gibbons and S. W. Hawking, “Cosmological event horizons, thermodynamics, and particle creation,” *Phys. Rev. D*, vol. 15, pp. 2738–2751, May 1977.
- [5] P. Davies, “Cosmological Event Horizons, Entropy and Quantum Particles,” *Ann. Inst. H. Poincaré Phys. Theor.*, vol. 49, p. 297, 1988.
- [6] T. Jacobson and R. Parentani, “Horizon entropy,” *Found. Phys.*, vol. 33, pp. 323–348, 2003.
- [7] P. Panangaden and R. M. Wald, “Probability distribution for radiation from a black hole in the presence of incoming radiation,” *Phys. Rev. D*, vol. 16, pp. 929–932, Aug 1977.
- [8] R. D. Sorkin, “On the Entropy of the Vacuum Outside a Horizon,” in *General Relativity and Gravitation, Volume 1* (B. Bertotti, F. de Felice, and A. Pascolini, eds.), vol. 1, p. 734, July 1983.
- [9] L. Bombelli, R. K. Koul, J. Lee, and R. D. Sorkin, “A Quantum Source of Entropy for Black Holes,” *Phys. Rev.*, vol. D34, pp. 373–383, 1986.
- [10] P. Calabrese and J. L. Cardy, “Entanglement entropy and quantum field theory,” *J. Stat. Mech.*, vol. 0406, p. P06002, 2004.

- [11] T. Jacobson and A. Satz, “Black hole entanglement entropy and the renormalization group,” *Phys. Rev.*, vol. D87, no. 8, p. 084047, 2013.
- [12] S. N. Solodukhin, “Entanglement entropy of black holes,” *Living Rev. Rel.*, vol. 14, p. 8, 2011.
- [13] R. Emparan, “Black hole entropy as entanglement entropy: A Holographic derivation,” *JHEP*, vol. 06, p. 012, 2006.
- [14] T. Jacobson, “Gravitation and vacuum entanglement entropy,” *Int. J. Mod. Phys. D*, vol. 21, p. 1242006, 2012.
- [15] T. Jacobson, “Black hole entropy and induced gravity,” 1994.
- [16] S. Ryu and T. Takayanagi, “Holographic derivation of entanglement entropy from the anti-de sitter space/conformal field theory correspondence,” *Physical Review Letters*, vol. 96, May 2006.
- [17] J. Maldacena and G. L. Pimentel, “Entanglement entropy in de sitter space,” *Journal of High Energy Physics*, vol. 2013, Feb 2013.
- [18] X. Dong, E. Silverstein, and G. Torroba, “De sitter holography and entanglement entropy,” *Journal of High Energy Physics*, vol. 2018, Jul 2018.
- [19] R. D. Sorkin, “Expressing entropy globally in terms of (4D) field-correlations,” *J. Phys. Conf. Ser.*, vol. 484, p. 012004, 2014.
- [20] Y. Chen, R. Kunjwal, H. Moradi, Y. K. Yazdi, and M. Zilhão, “Towards Spacetime Entanglement Entropy for Interacting Theories,” 2020.
- [21] M. Saravani, R. D. Sorkin, and Y. K. Yazdi, “Spacetime entanglement entropy in 1 + 1 dimensions,” *Class. Quant. Grav.*, vol. 31, no. 21, p. 214006, 2014.
- [22] S. Johnston, “Feynman Propagator for a Free Scalar Field on a Causal Set,” *Phys. Rev. Lett.*, vol. 103, p. 180401, 2009.
- [23] R. D. Sorkin, “From Green Function to Quantum Field,” *Int. J. Geom. Meth. Mod. Phys.*, vol. 14, no. 08, p. 1740007, 2017.
- [24] R. D. Sorkin and Y. K. Yazdi, “Entanglement Entropy in Causal Set Theory,” *Class. Quant. Grav.*, vol. 35, no. 7, p. 074004, 2018.
- [25] A. Belenchia, D. M. T. Benincasa, M. Letizia, and S. Liberati, “On the Entanglement Entropy of Quantum Fields in Causal Sets,” *Class. Quant. Grav.*, vol. 35, no. 7, p. 074002, 2018.
- [26] S. P. Johnston, *Quantum Fields on Causal Sets*. PhD thesis, Imperial Coll., London, 2010.
- [27] Nomaan X, F. Dowker, and S. Surya, “Scalar Field Green Functions on Causal Sets,” *Class. Quant. Grav.*, vol. 34, no. 12, p. 124002, 2017.

- [28] S. Surya, N. X, and Y. K. Yazdi, “Studies on the SJ Vacuum in de Sitter Spacetime,” *JHEP*, vol. 07, p. 009, 2019.
- [29] S. S. Abhishek Mathur, “The de sitter sj vacuum.” In preparation.
- [30] R. D. Sorkin and D. Sudarsky, “Large fluctuations in the horizon area and what they can tell us about entropy and quantum gravity,” *Class. Quant. Grav.*, vol. 16, pp. 3835–3857, 1999.
- [31] S. W. Hawking and G. F. R. Ellis, *The Large Scale Structure of Space-Time*. Cambridge Monographs on Mathematical Physics, Cambridge University Press, 1973.
- [32] R. Bousso, “Adventures in de Sitter space,” in *Workshop on the Future of Theoretical Physics and Cosmology in Honor of Hawking’s 60th*, pp. 539–569, 5 2002.
- [33] L. Bombelli, J. Lee, D. Meyer, and R. Sorkin, “Space-Time as a Causal Set,” *Phys. Rev. Lett.*, vol. 59, pp. 521–524, 1987.
- [34] F. Dowker, “Causal sets and the deep structure of spacetime,” in *100 Years Of Relativity: space-time structure: Einstein and beyond* (A. Ashtekar, ed.), pp. 445–464, 2005.
- [35] S. Surya, “The causal set approach to quantum gravity,” 2019.
- [36] S. Johnston, “Particle propagators on discrete spacetime,” *Class. Quant. Grav.*, vol. 25, p. 202001, 2008.
- [37] A. Chandran, C. Laumann, and R. D. Sorkin, “When is an area law not an area law?,” *Entropy*, vol. 18, p. 240, 2016.
- [38] J. Eisert, M. Cramer, and M. B. Plenio, “Area laws for the entanglement entropy - a review,” *Rev. Mod. Phys.*, vol. 82, pp. 277–306, 2010.
- [39] T. Garidi, “What is mass in de Sitterian physics?,” 2003.
- [40] N. Afshordi, M. Buck, F. Dowker, D. Rideout, R. D. Sorkin, and Y. K. Yazdi, “A Ground State for the Causal Diamond in 2 Dimensions,” *JHEP*, vol. 10, p. 088, 2012.
- [41] A. Mathur and S. Surya, “Sorkin-Johnston vacuum for a massive scalar field in the 2D causal diamond,” *Phys. Rev.*, vol. D100, no. 4, p. 045007, 2019.
- [42] M. Buck, F. Dowker, I. Jubb, and R. Sorkin, “The Sorkin–Johnston state in a patch of the trousers spacetime,” *Class. Quant. Grav.*, vol. 34, no. 5, p. 055002, 2017.
- [43] N. Afshordi, S. Aslanbeigi, and R. D. Sorkin, “A Distinguished Vacuum State for a Quantum Field in a Curved Spacetime: Formalism, Features, and Cosmology,” *JHEP*, vol. 08, p. 137, 2012.
- [44] B. Allen, “Vacuum States in de Sitter Space,” *Phys. Rev.*, vol. D32, p. 3136, 1985.

- [45] E. Mottola, “Particle creation in de sitter space,” *Phys. Rev. D*, vol. 31, pp. 754–766, Feb 1985.
- [46] B. Allen and A. Folacci, “The Massless Minimally Coupled Scalar Field in De Sitter Space,” *Phys. Rev.*, vol. D35, p. 3771, 1987.